PCCP

PAPER

View Article Online
View Journal | View Issue

Cite this: *Phys. Chem. Chem. Phys.*, 2022, **24**, 11820

Excluded volume interactions and phase stability in mixtures of hard spheres and hard rods

Joeri Opdam, †[a] Poshika Gandhi, †[b] Anja Kuhnhold, [b] Tanja Schilling ‡[b] and Remco Tuinier ‡*[a]

In this paper we study excluded volume interactions, the free volume fraction available, and the phase behaviour, in mixtures of hard spheres (HS) and hard rods, modeled as spherocylinders. We use free volume theory (FVT) to predict various physical properties and compare to Monte Carlo computer simulations. FVT is used at two levels. We use the original FVT approach in which it is assumed that the correlations of the HS are not affected by the rods. This is compared to a recent, more rigorous, FVT approach which includes excluded volume interactions between the different components at all levels. We find that the novel rigorous FVT approach agrees well with computer simulation results at the level of free volume available, as well as for the phase stability. The FVT predictions show significant quantitative and qualitative deviations with respect to the original FVT approach. The phase transition curves are systematically at higher rod concentrations than previously predicted. Furthermore, the calculations revealed that a certain asphericity is required to induce isostructural fluid–fluid coexistence and the stability region is highly dependent on the size ratio between the rods and the spheres.

Received 28th January 2022,
Accepted 6th April 2022

DOI: 10.1039/d2cp00477a

rsc.li/pccp

1 Introduction

Dense, multi-component mixtures of colloids and/or polymers are ubiquitous in systems such as paint,[1] food,[2] and a wide range of other technological applications. Paint is crowded with (associative) polymers, polymeric binder particles, and inorganic opacifiers such as colloidal titania. Food products typically contain high concentrations of proteins, polysaccharides, and/or emulsified oil droplets.[3]

Living matter also often contains highly concentrated dispersions of different types of biomacromolecules.[4] Bacterial cells, for instance, may contain a concentration of 0.3–0.4 g mL^{-1} of macromolecules[5,6] of different kinds and organisational structures such as the nucleus, nucleoli, or other compartments.[7,8] From a fundamental point of view, the different macromolecules interact through various types of forces. It is, thus, challenging to predict the physical properties for such complex mixtures. Excluded volume interactions are, however, nearly always present.

Asakura and Oosawa, in their two classical papers[9,10] on the binary mixtures of hard spheres (HS), discussed the existence of an attractive force between the big HS due to the presence of small HS. This attractive force is now referred to as the depletion interaction. Since in the 1970s and 1980s the focus was mainly on mixtures of colloids and nonadsorbing polymers, their work did not receive much attention for a long time.[11]

In the 1990s, however, work on the phase stability of binary HS mixtures gained a new impetus. Biben and Hansen[12] showed that there can be spinodal demixing in such mixtures, hinting at a possible colloidal gas–liquid phase separation (also referred to as fluid–fluid phase separation). Later, Stroobants and Lekkerkerker[13] developed a free volume theory (FVT) approach to predict the phase behaviour for these binary mixtures.

Generally in FVT two compartments at osmotic equilibrium are defined. One compartment is the system of interest that contains colloidal particles and depletants, while the second compartment is a hypothetical reservoir that only contains depletants. The compartments are connected through a membrane that is not permeable for the colloidal particles, but is permeable to the depletants. The solvent is treated as a background in FVT.

The FVT results of Stroobants and Lekkerkerker[13] demonstrated this gas–liquid phase separation is metastable and fluid–solid phase equilibria should be expected upon crossing the phase boundary. Dijkstra, van Roij and Evans[14] performed Monte Carlo computer simulations which confirmed this. Their simulations corresponded reasonably with FVT predictions,

[a] *Laboratory of Physical Chemistry, Department of Chemical Engineering and Chemistry, & Institute for Complex Molecular Systems (ICMS), Eindhoven University of Technology, P. O. Box 513, 5600 MB, Eindhoven, The Netherlands. E-mail: r.tuinier@tue.nl*
[b] *Institute of Physics, University of Freiburg, Hermann-Herder-Str. 3, 79104 Freiburg, Germany. E-mail: tanja.schilling@physik.uni-freiburg.de*
† These authors contributed equally to this work.
‡ These authors contributed equally to this work.

except for the solid–solid phase equilibria which appeared in the simulations but not in the FVT predictions.

Opdam *et al.*[15] improved the FVT approach by explicitly incorporating excluded volume interactions between the small HS depletants at all levels. The resulting FVT predictions were much closer to the computer simulations of Dijkstra *et al.*[14] and also predicted the solid–solid phase equilibria.

The pioneering work of Asakura and Oosawa[9,10] also revealed that rod-like particles are highly efficient depletants as their excluded volumes are relatively large. Mao, Cates and Lekkerkerker[16] derived analytical expressions to quantify the efficiency of hard rods and HS as depletants.

Vliegenthart and Lekkerkerker developed a version of FVT for the case of HS mixed with hard spherocylinders (HSC)[17] by means of a simple extension of the original FVT for HS with added ideal penetrable hard spheres (PHS).[18] This straightforward FVT[17] seems accurate for cases where the contribution of the excluded volume interactions between the rods is weak, as for the needle limit. It also enables to understand the main trends of computer simulations of HS and needles (infinitely thin rods)[19,20] and experimental studies of the phase stability of colloidal spheres mixed with rods.[21,22] Full scale simulations of HS and HSC are scarce[23–25] and do not report phase stability of the fluid–fluid or fluid–solid phase coexistence of HS as mediated by rod-like depletants.

Guu *et al.*[26] studied the phase behaviour of *fd*-virus and polystyrene spheres in aqueous salt solutions. Comparison with the FVT by Vliegenthart and Lekkerkerker[17] showed that FVT predicts phase transitions at too low colloidal rod concentrations.[27] More recently, it was shown that experimentally observed phase boundaries in mixtures of *fd*-virus and polystyrene spheres can be described more accurately by FVT with excluded volume interactions already included at the level of the reservoir.[27]

This novel FVT method is a relatively simple and quick method to predict the phase boundaries of colloidal mixtures. An accurate description of the phase behaviour may also help to predict and understand nucleation and crystallisation in such complex mixtures.[28] Here, we test the accuracy of the FVT by comparison with Monte Carlo simulations of dispersions containing HS mixed with HSC. First, we outline the FVT and simulation methods that were used. Next, we test the theoretical expressions used to describe the free volume available in a mixture of HSC and HS, which form the basis of the FVT calculations, against simulation results. Furthermore, we compare the boundaries for phase separation observed in the simulations with the phase diagrams obtained from both the original and the novel FVT predictions. Finally, we investigate the influence of the aspect ratio of HSC and the size ratio between the HSC and HS on the occurrence of isostructural fluid–fluid phase separation.

2 Methods

2.1 Free volume theory

Here, we outline the FVT employed in this paper, which is based on previous work on binary HS mixtures[15] but extended to take the anisotropic shape of rod-like depletants into account.[27] In FVT the two compartments used are in osmotic equilibrium and the thermodynamic properties of the system can be described by the semi-grand potential Ω. The experimental system of interest here is the mixture of hard spheres (s) and hard rod-like depletants (r). The system has a volume V, temperature T, and contains N_s spheres and N_r rods. It is assumed all interactions are hard: all HS and hard rods only interact through excluded volume interactions. The rods are described as hard spherocylinders, which are cylinders with volume v_r, length L and diameter D, capped by hemispheres with diameter D. The HS have a volume $v_s = 4\pi R^3/3$, with radius R. The dimensionless parameters describing the size ratio between the spheres and the rods are defined as

$$q = \frac{D}{2R}, \quad \xi = \frac{L}{R}. \tag{1}$$

The thermodynamic properties of the system are described using a semi-grand potential that reads:[27]

$$\widetilde{\Omega}_k = \widetilde{F}_{0,k} - \int_0^{\phi_d^R} \frac{\alpha_k^S(\phi_s, \phi_r)}{\alpha^R\left(\phi_r^{R'}\right)} \left(\frac{\partial \widetilde{\Pi}^R}{\partial \phi_r^{R'}}\right) \mathrm{d}\phi_r^{R'}. \tag{2}$$

where $\alpha_k^S(\phi_s, \phi_r)/\alpha^R(\phi_r^{R'})$ can be evaluated numerically by solving

$$\alpha^S(\phi_s, \phi_r) = \alpha^R\left(\phi_r^R\right) \frac{\phi_r}{\phi_r^R}, \tag{3}$$

for a given value of the rod concentration in the reservoir ϕ_r^R. Here α^R is the free volume fraction available for the HSC in the reservoir. In the original FVT,[17] $\alpha^R \equiv 1$. Here, however, we account for interactions between the HSC in the reservoir, so $\alpha^R < 1$ for $\phi_r^R > 0$. The quantity α^S is the free volume fraction available for the HSC in the system and depends both on the concentration of HSC in reservoir and system, and the concentration of HS in the system.

In eqn (2), k refers to the phase state of the HS which is, here, assumed to be either a fluid or a face-centered cubic (FCC) crystal. We used dimensionless quantities in eqn (2). The dimensionless quantities used in this paper are defined as:

$$\begin{aligned} \widetilde{\Omega} &= \frac{\Omega v_s}{V k_B T}, \quad \widetilde{F} = \frac{F v_s}{V k_B T}, \quad \widetilde{\Pi} = \frac{\Pi v_s}{k_B T}, \\ \widetilde{\mu} &= \frac{\mu}{k_B T}, \quad \alpha = \frac{\langle V_{free} \rangle}{V}, \quad \phi_i = \frac{N_i v_i}{V}, \end{aligned} \tag{4}$$

where i denotes either component s or r, v_i is the volume of component i, Π is the osmotic pressure, and α is the free volume fraction which is equal to the ensemble averaged free volume available for the depletants (rods) normalised by the total volume within a certain compartment.

For a fluid of hard spheres the free energy is approximated using the Carnahan–Starling equation of state:[29]

$$\widetilde{F}_{0,fluid} = \phi_s\left[\ln\left(\phi_s \Lambda^3 / v_s\right) - 1\right] + \frac{4\phi_s^2 - 3\phi_s^3}{(1-\phi_s)^2}, \tag{5}$$

where Λ is the de Broglie wavelength. The free energy of the

pure HS FCC crystal phase is described using cell theory as:[30]

$$\widetilde{F}_{0,\mathrm{solid}} = \phi_\mathrm{s}\ln\left(\Lambda^3/v_\mathrm{s}\right) + \phi_\mathrm{s}\ln\left(\frac{27}{8\phi_\mathrm{cp}^3}\right) + 3\phi_\mathrm{s}\ln\left(\frac{\phi_\mathrm{s}}{1-\phi_\mathrm{s}/\phi_\mathrm{cp}}\right). \quad (6)$$

Here, the volume fraction of a close-packed FCC crystal is $\phi_\mathrm{cp} = \pi/(3\sqrt{2})$.

For the HSC concentrations used in this work it is assumed that the rod-like particles only adopt isotropic configurations.[31,32] We use scaled particle theory (SPT) to quantify the osmotic pressure of a fluid of HSC[33] in the reservoir:

$$\widetilde{\Pi}^\mathrm{R} = \frac{v_\mathrm{s}}{v_\mathrm{r}}\left[\frac{\phi_\mathrm{r}^\mathrm{R}}{1-\phi_\mathrm{r}^\mathrm{R}} + \frac{3\gamma(\gamma+1)}{3\gamma-1}\left(\frac{\phi_\mathrm{r}^\mathrm{R}}{1-\phi_\mathrm{r}^\mathrm{R}}\right)^2 + \frac{12\gamma^3}{(3\gamma-1)^2}\left(\frac{\phi_\mathrm{r}^\mathrm{R}}{1-\phi_\mathrm{r}^\mathrm{R}}\right)^3\right]. \quad (7)$$

The dimensionless parameter γ is related to the aspect ratio of the rods L/D as:

$$\gamma = 1 + \frac{L}{D}. \quad (8)$$

In a binary mixture of HS and HSC with total volume fraction $\phi = \phi_\mathrm{s} + \phi_\mathrm{r}$, the free volume fraction available to a HSC can be determined with scaled particle theory:[27]

$$\alpha^\mathrm{S} = (1-\phi)\exp\left[-\tau\frac{\phi}{1-\phi} - \Upsilon\left(\frac{\phi}{1-\phi}\right)^2 - \frac{v_\mathrm{r}}{v_\mathrm{s}}\widetilde{\Pi}^\mathrm{SPT}\right], \quad (9)$$

with

$$\tau = \left[\frac{3}{4}\xi(1+2q) + 3q(1+q)\right]\frac{\phi_\mathrm{s}}{\phi} + \left[6 + \frac{6(\gamma-1)^2}{3\gamma-1}\right]\frac{\phi_\mathrm{r}}{\phi}. \quad (10)$$

$$\Upsilon = \left[\left(\frac{3}{4}\xi + \frac{3}{2}q\right)\frac{\phi_\mathrm{s}}{\phi} + \frac{3\gamma^2}{3\gamma-1}\frac{\phi_\mathrm{r}}{\phi}\right]\left(3q\frac{\phi_\mathrm{s}}{\phi} + \frac{6\gamma}{3\gamma-1}\frac{\phi_\mathrm{r}}{\phi}\right). \quad (11)$$

where $\tilde{\Pi}^\mathrm{SPT}$ refers to the SPT expression for the osmotic pressure of the binary HS + HSC system:[34]

$$\widetilde{\Pi}^\mathrm{SPT} = \left(\phi_\mathrm{s} + \frac{v_\mathrm{s}}{v_\mathrm{r}}\phi_\mathrm{r}\right)\left[\frac{1}{1-\phi} + \frac{\Psi}{2}\frac{\phi}{(1-\phi)^2} + \frac{2}{3}\Theta\frac{\phi^2}{(1-\phi)^3}\right], \quad (12)$$

with:

$$\Psi = \frac{\kappa-\tau}{1+\frac{\phi_\mathrm{r}v_\mathrm{s}}{\phi_\mathrm{s}v_\mathrm{r}}} + \tau, \quad (13)$$

$$\Theta = \frac{\iota-\Upsilon}{1+\frac{\phi_\mathrm{r}v_\mathrm{s}}{\phi_\mathrm{s}v_\mathrm{r}}} + \Upsilon, \quad (14)$$

$$\kappa = 6\frac{\phi_\mathrm{s}}{\phi} + \frac{1}{q^2}\left[\frac{6q\gamma + 3(\gamma+1)}{3\gamma-1}\right]\frac{\phi_\mathrm{r}}{\phi}, \quad (15)$$

$$\iota = \frac{1}{2}\left(3\frac{\phi_\mathrm{s}}{\phi} + \frac{6\gamma}{q(3\gamma-1)}\frac{\phi_\mathrm{r}}{\phi}\right)^2. \quad (16)$$

With this SPT approach for the free volume available to a HSC, no distinction is made between a fluid or solid phase of the spheres in eqn (9) except for the difference in volume fraction. The free volume fraction in the reservoir α^R can be determined with eqn (9) by stating $\phi_\mathrm{s} = 0$.

Colloidal fluid–fluid and fluid–solid binodals of the mixture of HS and HSC are determined through the equilibrium conditions

$$\widetilde{\mu}_\mathrm{s}^\mathrm{G} = \widetilde{\mu}_\mathrm{s}^\mathrm{L}, \quad (17)$$

$$\widetilde{\Pi}^\mathrm{G} = \widetilde{\Pi}^\mathrm{L}, \quad (18)$$

for gas–liquid phase coexistence and

$$\widetilde{\mu}_\mathrm{s}^\mathrm{F} = \widetilde{\mu}_\mathrm{s}^\mathrm{S}, \quad (19)$$

$$\widetilde{\Pi}^\mathrm{F} = \widetilde{\Pi}^\mathrm{S}, \quad (20)$$

for fluid–solid equilibria. The superscript G denotes the colloidal gas phase, superscript L the colloidal liquid phase, superscript F the colloidal fluid phase, and superscript S identifies the colloidal solid phase. The three-phase G–L–S coexistence region is found by combining eqn (17)–(20). The critical point of gas–liquid coexistence is found by solving

$$\left(\frac{\partial\widetilde{\mu}_\mathrm{s}}{\partial\phi_\mathrm{s}}\right)_{\widetilde{\Pi}^\mathrm{R},V,T} = \left(\frac{\partial^2\widetilde{\mu}_\mathrm{s}}{\partial\phi_\mathrm{s}^2}\right)_{\widetilde{\Pi}^\mathrm{R},V,T} = 0. \quad (21)$$

The chemical potential of the spheres $\mu_\mathrm{s} = (\partial\Omega/\partial n_\mathrm{s})_{\Pi^\mathrm{R},V,T}$ and the osmotic pressure $\Pi = (\partial\Omega/\partial V)_{\Pi^\mathrm{R},ns,T}$, where n_s is the number of colloidal hard spheres, are related to the semi-grand potential given by eqn (2):

$$\widetilde{\mu}_\mathrm{s} = \left(\frac{\partial\widetilde{\Omega}}{\partial\phi_\mathrm{s}}\right)_{\widetilde{\Pi}^\mathrm{R},V,T}, \quad (22)$$

$$\widetilde{\Pi} = -\left(\frac{\partial(\widetilde{\Omega}/\phi_\mathrm{s})}{\partial(1/\phi_\mathrm{s})}\right)_{\widetilde{\Pi}^\mathrm{R},n_\mathrm{s},T} = \phi_\mathrm{s}\widetilde{\mu}_\mathrm{s} - \widetilde{\Omega}. \quad (23)$$

Coexistence densities and critical points were obtained by solving the equations presented in this section with a numerical scheme. The details for this procedure are given in Appendix A.

2.2 Simulations

We use Metropolis Monte Carlo (MC) simulations to study the phase behaviour of and the free volume in mixtures of HS and HSC (also referred to as rods). The relevant parameters that describe these objects are defined in Section 2.1. Fig. 1 shows a sketch of the simulated system. Initial configurations are set up by having a (simple cubic) lattice of HS as a central layer, sandwiched between layers of HSC. The rods initially point normal to the HS/HSC interface. The number of particles and

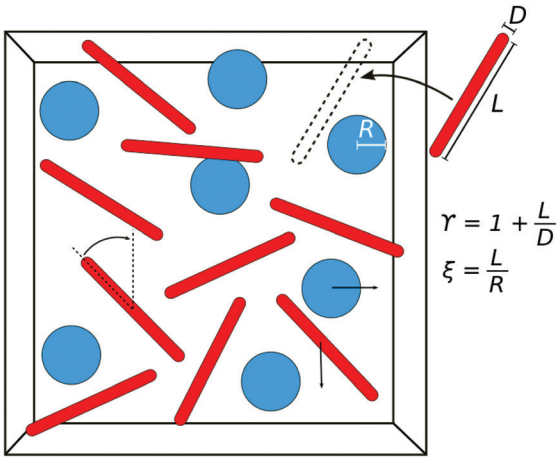

Fig. 1 Sketch of the simulated system. Spherocylinders ("rods" have length L and diameter D and spheres have radius R. Spheres and rods do translational moves and rods also do rotational moves (indicated by small arrows). To estimate the free volume available for spherocylinders trial insertion moves are executed (indicated by a rod that is moved from outside the box to the position of the dashed rod inside the box).

the volume of the simulation box are fixed for each set of parameters, and we use single-particle moves to relax the system towards its equilibrium state. These moves are random translations within a cube of length d_m^s (d_m^r) around the current position for the spheres (rods), and random rotations within a cone of opening angle γ_m^r around the current orientation for the rods. A move is accepted when it does not lead to an overlap between the moved particle and any other particle in the system, otherwise it is rejected. The parameters d_m^s, γ_m^r, and d_m^r are adjusted to give acceptance rates close to 0.5 for each of the move types. To equilibrate the systems, at least 2×10^5 MC sweeps are carried out. We evaluated the nematic order parameter of the rods and the acceptance rates of the moves to judge the equilibration process, and increased the number of MC sweeps if necessary. We also checked that the spheres had moved a distance larger than their diameter (if not in the solid state) from their initial positions. The resulting phases are identified by measuring relevant order parameters during the production sweeps and by visual inspection of the particle distribution in the simulation box. The simulation box with periodic boundary conditions is either cubic (below called symmetric) or cuboidal with a square cross section (below called asymmetric). The latter is used for simulations close to the phase separation points in order to reduce the size of the interface between two phases. For the simulation results presented in this paper, we use up to $N_s = 625$ HS and up to $N_r = 20\,000$ HSC.

To estimate the free volume fraction available for the rods, we measure the acceptance rate of trial insertions of a rod into the system: $\alpha^S \approx \langle n_{acc}^i / n_{trial}^i \rangle$, where n_{trial}^i is the number of trial insertions of a rod with arbitrary orientation at an arbitrary position, and n_{acc}^i is the number of accepted insertions. (Note that the insertion is only temporary; the number of rods is kept constant by removing the inserted rod.) The angular brackets denote the canonical ensemble average for which 1000 configurations (out of 1×10^5 MC sweeps) are used with $n_{trial}^i = 1000$ per configuration.

3 Results and discussion

3.1 Free volume fraction

First the free volume theory (FVT), including excluded volume interactions accounted for at the reservoir level, is tested *versus* the computer simulation results by evaluating the free volume fraction in the system. The free volume fraction available to the hard spherocylinder (HSC) depletants in the binary mixture, α^S, is determined using scaled particle theory (eqn (9)) and depends on the volume fraction of both components, the size ratios $L/R = \xi$ and $D/(2R) = q$, and the HSC aspect ratio $\gamma = L/D + 1$. Note that $\xi = 2q(\gamma - 1)$, so there are only two independent parameters that describe the size ratios and aspect ratio. In Fig. 2 results are plotted for the free volume fraction in the system α^S as a function of the volume fraction of HSC (ϕ_r) for various values of ϕ_s (a), γ (b) and ξ (c). The solid curves are FVT

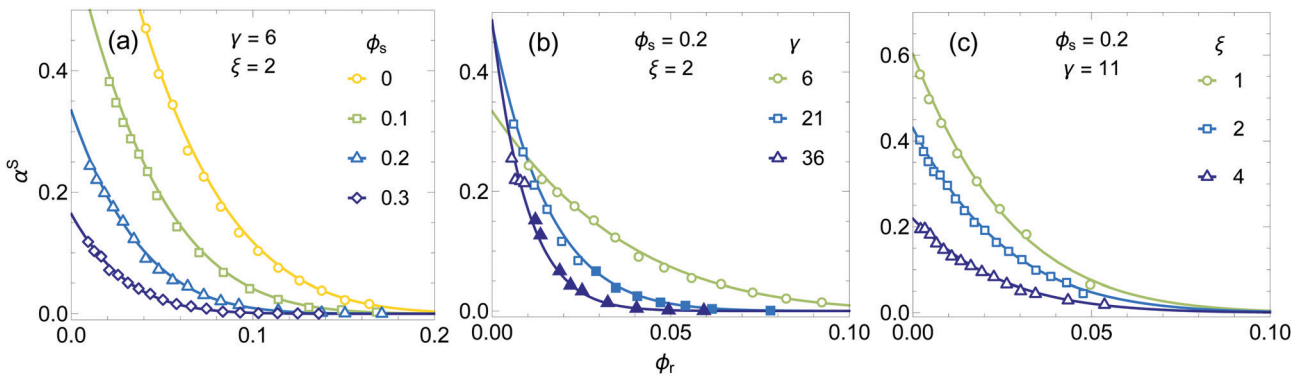

Fig. 2 Free volume fraction α^S for HSC in a mixture of HSC and HS as a function of rod volume fraction ϕ_r. The curves show the SPT predictions from eqn (9) and the symbols show Monte Carlo computer simulation results. The parameters that are investigated are the sphere volume fraction ϕ_s (a), the aspect ratio $\gamma = L/D + 1$ (b) and the size ratio $\xi = L/R$ (c). The sphere volume fractions used for the calculations match the ones from the simulations (values for ϕ_s in the insets are rounded). Open symbols are used for homogeneous systems and closed symbols indicate phase separated systems. The numbers of HS and HSC used in the simulations range from $N_s = 100$ to 625 and from $N_r = 32$ to 20 000.

predictions, while the symbols are Monte Carlo computer simulation results.

There is good agreement between the theoretical predictions for the free volume fraction and the simulation results for all the parameters considered. The open symbols in Fig. 2 correspond to homogeneous mixtures, whereas phase separation was observed for the mixtures corresponding to the closed symbols. Surprisingly, although the theoretical predictions should only hold for homogeneous mixtures, the free volume fractions in the phase separated systems also follow the theoretical predictions very well. It is noted that in the original FVT, the free volume available in both the reservoir and the system is independent of the rod concentration, which is clearly not the case as seen in Fig. 2.

Fig. 2b and c show that the dependency of the HSC aspect ratio γ and the size ratio ξ on the free volume available to a HSC in a HS/HSC mixture is accurately described by SPT. Hence, eqn (9) is accurate which means that the distribution of depletants over the system and the reservoir, given by the ratio of the free volume fraction in the system and the reservoir (corresponding to $\phi_s = 0$ in Fig. 2a), can now be accurately incorporated into free volume theory.

It is noted that the results in Fig. 2 are for a fluid phase. Ordering of particles can not be accurately accounted for by SPT and therefore the predictions for the free volume in a solid phase are expected to be less accurate. Furthermore, any effect of local ordering or fluctuations in particle concentrations is not incorporated in FVT, whereas this is accounted for in the simulations. The results in Fig. 2 suggest that this theoretical approximation yields an accurate description for the free volume in the fluid phase.

3.2 Phase behaviour

In Fig. 3 we plot phase diagrams from FVT and phase state points from MC simulations for a size ratio of $\xi = 2$ and three different values of γ; 6, 21 and 36, corresponding to the parameters in Fig. 2b. The grey curves are the predictions of the original FVT,[17] whereas results from the new FVT, that includes excluded volume interactions at the reservoir level,[27] are plotted as the black curves. The dashed curve in panel (b) indicates that fluid–fluid (FF) coexistence is metastable with respect to fluid–solid (FS) coexistence. The blue symbols show the simulation data, open symbols denote a homogeneous binary fluid was obtained and closed symbols denote phase separation was observed.

A substantial quantitative and qualitative deviation can be seen between the phase transition concentrations predicted by the two different FVT approaches. The homogeneous fluid phase region is much larger when the excluded volume interactions at all levels (black curves) are accounted for. The original FVT of Vliegenthart and Lekkerkerker predicts a stable region of FF demixing and a corresponding three-phase fluid–fluid–solid coexistence region for all three considered aspect ratios. The new FVT approach predicts that the FF demixing is metastable with respect to FS coexistence at small aspect ratios. Only for the largest value of $\gamma = 36$ a stable FF coexistence region is found. When the aspect ratio increases, the deviation between the two FVT approaches becomes smaller, as expected, since both methods are equal in the limit of infinitely thin rods ($\gamma \to \infty$). Overall, the data points from MC simulations support the predicted phase transitions from the new FVT, as they are in much better agreement.

There are some small deviations between the theoretical predictions and the simulation results which can be expected due to the approximations in the theoretical model. The main simplifications in the theory are in the free volume descriptions, which are determined with SPT for both the fluid phase and the solid phase. The finite size of the simulation box might also result in a slight difference between the simulation results and FVT predictions. The coexisting phases in the simulation box have a finite size with a limited number of particles, separated by an interface. The formation of this interface might

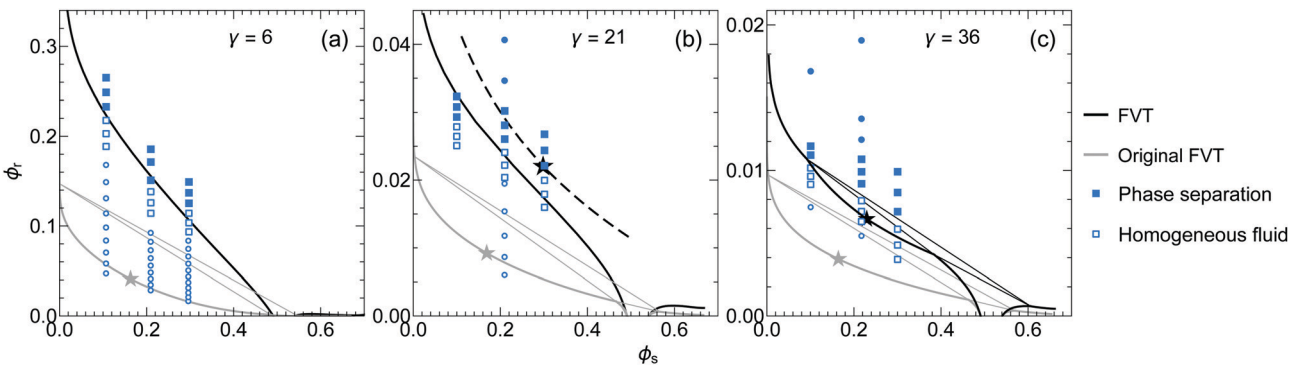

Fig. 3 Phase diagrams of HSC/HS mixtures with a size ratio $\xi = L/R = 2$ and HSC aspect ratios $\gamma = L/D + 1$ of 6 (a), 21 (b) and 36 (c). The black curves show the FVT calculations and the grey curves show the predictions for the original FVT of Vliegenthart and Lekkerkerker.[17] The star symbol denotes the fluid–fluid (FF) critical point and the dashed curve in panel (b) indicates that FF demixing is metastable. The triangular areas show the borders of the three-phase fluid–fluid–solid coexistence region. The blue symbols show the simulation results. An open symbol indicates a homogeneous binary fluid was obtained and a closed symbol means phase separation occurred. The square symbols show results obtained with an asymmetric simulation box and the round symbols show results from a symmetric simulation box. The numbers of HS and HSC used in the simulations range from $N_s = 121$ to 625 and from $N_r = 1250$ to 14 112.

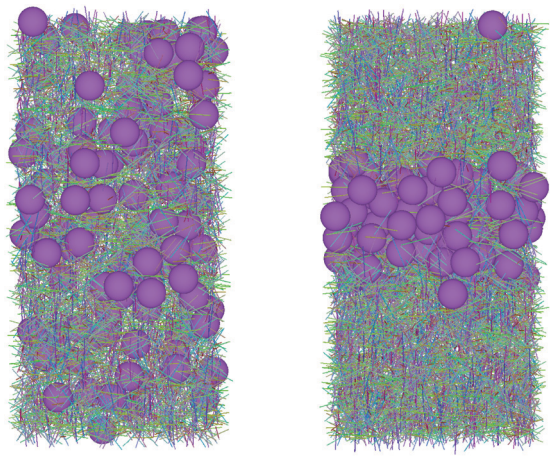

Fig. 4 Representative snapshots for homogeneous and phase separated systems. The HSC/HS size ratio is $\xi = L/R = 2$, the HSC aspect ratio is $\gamma = L/D + 1 = 36$, the sphere volume fraction is $\phi_s = 0.1$, and the rod volume fractions are $\phi_r = 0.008$ (left) and 0.012 (right). The respective numbers of HS and HSC are $N_s = 121$, and $N_r = 7688$ (left) and 11 250 (right).

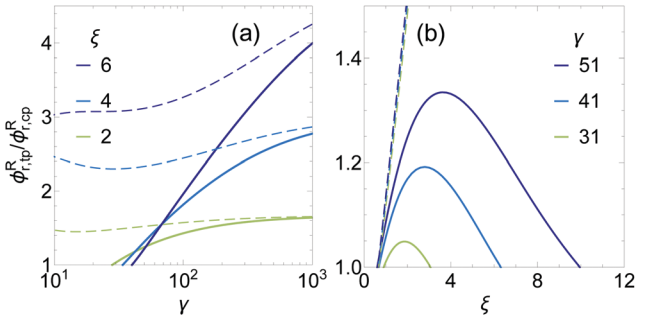

Fig. 5 Relative size of the fluid–fluid phase coexistence region given by the ratio of the rod volume fraction in the reservoir between the triple point and the critical point as a function of $\gamma = L/D + 1$ for different size ratios $\xi = L/R$ (a) and as a function of ξ for different aspect ratios γ (b). A critical value of γ or ξ is found when the ratio $\phi^R_{r,tp}/\phi^R_{r,cp}$ equals 1 (*i.e.* the critical end point). The solid curves show the FVT results and the dashed curves show the results for the original FVT of Vliegenthart and Lekkerkerker.[17]

result in a slightly stronger depletion interaction, thus a higher rod concentration, needed to induce phase separation. Verifying the type of coexisting phases with the MC simulations is complicated since the formation of a solid phase might be affected by the limited number of spherical particles in the system, which prevents the formation of a large macroscopic crystalline phase. Especially for large aspect ratios, the number of rods in the system is much greater than the number of spheres and therefore, this increase in the number of spheres in the simulation box results in very long computation times. Representative snapshots of configurations obtained with MC simulations for both a homogeneous system and a phase separated system, with $\gamma = 36$ and $\phi_s = 0.1$, are shown in Fig. 4. The transition from a homogeneous mixture of spheres and rods, to a phase separated system can be clearly observed in the two systems where the difference in rod volume fraction is only 0.004.

3.3 Stability regions of fluid–fluid coexistence

For $L/D = 0$ ($\gamma = 1$), HSC have a spherical shape. For binary HS mixtures, it has been shown that FF coexistence is metastable for all size ratios.[15] The results in Fig. 3 reveal that FF is predicted to become stable for sufficiently large γ. Therefore, it is expected that a certain asphericity is required to stabilize a FF demixing region. For this reason, at a certain given size ratio ξ, there should be a critical aspect ratio γ above which there is a stable FF coexistence region in the phase diagram of a HSC/HS mixture. Fig. 5a shows the ratio of the HSC reservoir volume fraction ϕ^R_r between the triple FFS coexistence region and the FF critical point as a function of γ for different size ratios ξ. This ratio is a measure for the relative size of the FF region (the liquid window) in the phase diagram. When this ratio equals unity, the FF critical point touches the FS coexistence lines and the three phase coexistence region disappears. The set of parameters where this occurs is denoted as the critical end point (CEP).

The solid curves in Fig. 5 show the results from the FVT as outlined in Section 2.1 and, as expected, predict that a CEP is found at a certain aspect ratio (γ^*) for FF demixing in HSC/HS mixtures. For $2 \leq \xi \leq 6$ we find $30 \lesssim \gamma^* \lesssim 40$, corroborating the trends of Fig. 3. This confirms that a certain HSC asphericity is required to stabilize FF coexistence in hard colloidal mixtures. The dashed curves in Fig. 5 show the original FVT predictions. The results are similar for large aspect ratios, however, for smaller aspect ratios the two FVT approaches significantly deviate and no CEP is found for the dashed curves.

The exact value of γ^* depends on the size ratio ξ and for the size ratios considered, γ^* increases as a function of ξ. This indicates that for a certain value of γ there should also be a corresponding critical size ratio ξ above which FF coexistence becomes metastable. However, it is also known that when the HSC become small with respect to the HS, FF coexistence becomes metastable. This means that there should be two critical values of ξ in between which there is a stable FF coexistence region. This is indeed found in the FVT predictions, as can be seen in Fig. 5b that shows the ratio $\phi^R_{r,tp}/\phi^R_{r,cp}$ as a function of ξ for different HSC aspect ratios γ.

This result suggests that if either component in a binary colloidal mixture becomes too large with respect to the other component, FF coexistence becomes metastable. Verification of the trends of the thermodynamic stability of the FF coexistence regions as a function of the aspect ratio and size ratio with simulations or experiments is desired. However, due to the computation times for mixtures of HS and HSC with large aspect ratios, this is a difficult task with simulations. Also, experimentally it is challenging to find a proper model system where a large parameter space can be investigated and analysis of the composition of coexisting phases in an experimental system can be demanding.

The lower critical value of ξ is approximately 0.6 for large aspect ratios, which is similar to the critical size ratio found for

infinitely thin rods by Bolhuis and Frenkel[19] and for rods with γ = 21 found by Vliegenthart and Lekkerkerker with original FVT.[17] For small aspect ratios, close to γ^*, the lower critical ξ^* slightly increases. The upper critical ξ^* increases significantly as a function of aspect ratio, and also the maximum size of the FF coexistence region, found at intermediate size ratios, becomes larger for more anisotropic HSC. The original FVT predictions are again shown by the dashed curves and show very different behaviour. The size of the FF region is significantly larger in the original predictions and no upper critical ξ^* is observed. Moreover, the effect of the aspect ratio is much weaker in the original predictions.

It should be noted that in these calculations only the ordered phase for the HS particles is considered, whereas the ordered phases for the HSC particles are not included. For certain parameters it could be possible that the fluid phases in the three phase region are not in equilibrium with a solid phase, but with a phase where the HSC are ordered, for example the nematic phase. HSC already display a rich phase behaviour as a function of their aspect ratio[32] and when mixed with polymeric depletants, FVT predicts a wide variety of stable multiphase coexistence regions.[35] Until now, the phase behaviour of HSC with HS as depletants, as well as the phase behaviour of HS with HSC have been considered with FVT. However, phase diagrams where the excluded volume of both components is explicitly accounted for and where both particles can form ordered phases have not been reported with FVT. For future work it will be of interest to determine the complete phase stability map of HSC/HS mixtures that takes into account ordering of both components. This will potentially reveal new types of multiphase coexistence regions that have not yet been reported.

4 Conclusions

The accuracy of free volume theory (FVT) that explicitly accounts for the excluded volume of depletants was verified for mixtures of hard spherocylinders (HSC) and hard spheres (HS) using Monte Carlo simulations. Both FVT predictions for the free volume available in HSC/HS mixtures and the phase boundaries of such mixtures were compared and good agreement was found with the simulations for the parameters considered. Theoretical predictions using the original FVT approach, where the excluded volume of the HSC particles is neglected in the expressions for the free volume fraction, deviate substantially from the new FVT and the simulation results. The results show that accurately accounting for the excluded volume of all components is key in mapping the phase behaviour of colloidal mixtures.

FVT was used to map the phase stability region for isostructural fluid–fluid coexistence as a function of the HSC aspect ratio $\gamma = L/D + 1$ and the size ratio $\xi = L/R$. In contrast to original FVT predictions, the new FVT method predicts a critical aspect ratio γ^* below which fluid–fluid (FF) coexistence is metastable with respect to fluid–solid coexistence. This critical aspect ratio is expected because it has been shown that FF coexistence is metastable in binary hard-sphere mixtures for all size ratios[15] and HSC particles reduce to spheres in the limit of $\gamma \to 1$. Moreover, FVT predicts that for a certain aspect ratio, there is not only a lower critical size ratio $\xi^* \approx 0.6$ below which FF coexistence becomes metastable, but also an upper critical size ratio ξ^* above which FF coexistence is metastable. This indicates that fluid–fluid demixing becomes metastable in binary colloidal mixtures if either component becomes relatively large with respect to the other component.

Conflicts of interest

There are no conflicts to declare.

Appendix

A Numerical scheme for phase coexistence calculations

Coexistence densities for specific size ratios q and ξ were determined by solving eqn (17) and (18) (G–L coexistence) or eqn (19) and (20) (F–S coexistence) with a numerical scheme. First the distribution of the rod-like depletants between the reservoir and the system is numerically determined by solving eqn (3) for a range of reservoir volume fractions ϕ_r^R. The resulting data is interpolated and used as input to determine $\widetilde{\Omega}$ for a given volume fraction of spherical particles ϕ_s and a given ϕ_r^R. These steps are repeated for a range of sphere volume fractions and again interpolation was used to obtain $\widetilde{\Omega}$ as a function of ϕ_s which is used as input for eqn (17)–(23). Binodals are finally obtained by repeating this scheme for different values of ϕ_r^R, which can be converted to the volume fraction of rods in the system ϕ_r using eqn (3).

F-F critical points and three-phase coexistence regions were obtained by determining $\widetilde{\Pi}^F$, $\widetilde{\Pi}^S$, $\widetilde{\mu}_s^F$, $\widetilde{\mu}_s^S$, $\left(\partial\widetilde{\mu}_s^F/\partial\phi_s\right)_{\widetilde{\Pi}^R,V,T}$ and $\left(\partial^2\widetilde{\mu}_s^F/\partial{\phi_s}^2\right)_{\widetilde{\Pi}^R,V,T}$ for a range of sphere volume fractions ϕ_s and reservoir rod volume fractions ϕ_r^R. The obtained results were interpolated as a function of ϕ_s and ϕ_r^R and the critical points were finally determined with eqn (21). The three-phase coexistence region was found by solving eqn (17)–(20). All calculations were done using Wolfram Mathematica 12.

Acknowledgements

J. O. and R. T. acknowledge financial support from the Dutch Ministry of Economic Affairs of the Netherlands *via* the Top Consortium for Knowledge and Innovation (TKI) roadmap Chemistry of Advanced Materials (Grant No. CHEMIE.PGT.2018.006). P. G. and A. K. acknowledge financial support from the German Research Foundation (DFG, Project-ID 435320238). Support by the state of Baden-Württemberg through bwHPC and the German Research

Foundation (DFG) through grant no INST 39/963-1 FUGG (bwForCluster NEMO) is acknowledged.

References

1 G. de With, *Polymer Coatings*, Wiley, New York, 2018.
2 P. Walstra, *Physical Chemistry of Foods*, Marcel Decker, New York, 2003.
3 A. Syrbe, W. J. Bauer and H. Klostermeyer, *Int. Dairy J.*, 1998, **8**, 179–193.
4 A. A. M. André and E. Spruijt, *Int. J. Mol. Sci.*, 2020, **21**, 5908.
5 D. S. Goodsell, *The Machinery of Life*, Springer, New York, 1998.
6 D. Marenduzzo, K. Finan and P. R. Cook, *J. Cell Biol.*, 2006, **175**, 681–686.
7 H. Walter and D. E. Brooks, *FEBS Lett.*, 1995, **361**, 135–139.
8 C. L. Woldringh and T. Odijk, in *Organization of the Prokaryotic Genome*, ed. R. L. Charlebois, ASM Press, Amsterdam, 1999, ch. 10.
9 S. Asakura and F. Oosawa, *J. Chem. Phys.*, 1954, **22**, 1255–1256.
10 S. Asakura and F. Oosawa, *J. Polym. Sci.*, 1958, **33**, 183–192.
11 K. Kurihara and B. Vincent, *J. Chem. Phys.*, 2021, **154**, 220401.
12 T. Biben and J.-P. Hansen, *Phys. Rev. Lett.*, 1991, **66**, 2215–2218.
13 H. N. W. Lekkerkerker and A. Stroobants, *Physica A*, 1993, **195**, 387–397.
14 M. Dijkstra, R. Van Roij and R. Evans, *Phys. Rev. E: Stat. Phys., Plasmas, Fluids, Relat. Interdiscip. Top.*, 1999, **59**, 5744–5771.
15 J. Opdam, M. P. M. Schelling and R. Tuinier, *J. Chem. Phys.*, 2021, **154**, 074902.
16 Y. Mao, M. E. Cates and H. N. W. Lekkerkerker, *J. Chem. Phys.*, 1997, **106**, 3721–3729.
17 G. A. Vliegenthart and H. N. W. Lekkerkerker, *J. Chem. Phys.*, 1999, **111**, 4153–4157.
18 H. N. W. Lekkerkerker, W. C. K. Poon, P. N. Pusey, A. Stroobants and P. B. Warren, *Europhys. Lett.*, 1992, **20**, 559–564.
19 P. Bolhuis and D. Frenkel, *J. Chem. Phys.*, 1994, **101**, 9869–9875.
20 S. C. McGrother, D. C. Williamson and G. Jackson, *J. Chem. Phys.*, 1996, **104**, 6755–6771.
21 G. A. Vliegenthart, A. van Blaaderen and H. N. W. Lekkerkerker, *Faraday Discuss.*, 1999, **112**, 173–182.
22 G. H. Koenderink, S. Sacanna, D. G. A. L. Aarts and A. P. Philipse, *Phys. Rev. E: Stat., Nonlinear, Soft Matter Phys.*, 2004, **69**, 021804.
23 T. Koda, M. Numajiri and S. Ikeda, *J. Phys. Soc. Jpn.*, 1996, **65**, 3551–3556.
24 T. Koda and S. Ikeda, *J. Chem. Phys.*, 2002, **116**, 5825–5830.
25 L. Wu, A. Malijevský, G. Jackson, E. A. Müller and C. Avendano, *J. Chem. Phys.*, 2015, **143**, 044906.
26 D. Guu, J. K. G. Dhont, G. A. Vliegenthart and M. P. Lettinga, *J. Phys.: Condens. Matter*, 2012, **24**, 464101.
27 J. Opdam, D. Guu, M. P. M. Schelling, D. G. A. L. Aarts, R. Tuinier and M. P. Lettinga, *J. Chem. Phys.*, 2021, **154**, 204906.
28 J. A. Wood, Y. Liu and A. Widmer-Cooper, *J. Chem. Phys.*, 2021, **154**, 244505.
29 N. F. Carnahan and K. E. Starling, *J. Chem. Phys.*, 1969, **51**, 635–636.
30 J. E. Lennard-Jones and A. F. Devonshire, *Proc. R. Soc. A*, 1937, **163**, 53–70.
31 P. Bolhuis and D. Frenkel, *J. Chem. Phys.*, 1997, **106**, 666–687.
32 V. F. D. Peters, M. Vis, H. H. Wensink and R. Tuinier, *Phys. Rev. E*, 2020, **101**, 062707.
33 M. A. Cotter, *Phys. Rev. A: At., Mol., Opt. Phys.*, 1974, **10**, 625–636.
34 M. F. Holovko and M. V. Hvozd, *Condens. Matter Phys.*, 2017, **20**, 43501.
35 V. F. D. Peters, M. Vis, Á. González García, H. H. Wensink and R. Tuinier, *Phys. Rev. Lett.*, 2020, **125**, 127803.